Available online at www.sciencedirect.com
ScienceDirect
Trans. Nonferrous Met. Soc. China 27(2017) 2647−2655
Transactions of Nonferrous Metals Society of China
www.tnmsc.cn

Shape memory TiNi powders produced by plasma rotating electrode process for additive manufacturing

Gang CHEN[1,2], Shao-yang ZHAO[1], Ping TAN[1], Jing-ou YIN[1], Quan ZHOU[1,3], Yuan GE[1], Zeng-feng LI[1], Jian WANG[1], Hui-ping TANG[1,4], Peng CAO[5]

1. State Key Laboratory of Porous Metal Materials, Northwest Institute for Non-ferrous Metal Research, Xi'an 710016, China;
2. State Key Laboratory of Powder Metallurgy, Central South University, Changsha 410083, China;
3. School of Materials Science and Engineering, Northeastern University, Shenyang 110819, China;
4. Xi'an Sailong Metal Materials Co., Ltd., Xi'an 710016, China;
5. Department of Chemical and Materials Engineering, The University of Auckland, Private Bag 92019, Auckland 1142, New Zealand

Received 21 February 2017; accepted 5 June 2017

Abstract: This study aimed to produce spherical TiNi powders suitable for additive manufacturing by plasma rotating electrode process (PREP). Scanning electron microscopy, X-ray diffractometry and differential scanning calorimetry were used to investigate the surface and inner micro-morphology, phase constituent and martensitic transformation temperature of the surface and inner of the atomized TiNi powders with different particle sizes. The results show that the powder surface becomes smoother and the grain becomes finer gradually with decreasing particle size. All the powders exhibit a main *B*2-TiNi phase, while large powders with the particle size ≥178 μm contain additional minor Ti_2Ni and Ni_3Ti secondary phases. These secondary phases are a result of the eutectoid decomposition during cooling. Particles with different particle sizes have experienced different cooling rates during atomization. Various cooling rates cause different martensitic transformation temperatures and routes of the TiNi powders; in particular, the transformation temperature decreases with decreasing particle size.

Key words: atomization; plasma rotating electrode process; TiNi; particle size; martensitic transformation

1 Introduction

The equiatomic TiNi shape memory alloy was first discovered by BUEHLER et al [1] accidentally. Since its discovery, TiNi alloy has been attracting continuous research interest due to its unique properties such as shape memory effect, good corrosion resistance and good biocompatibility [2]. Recently, additive manufacturing (AM) such as selective laser melting (SLM) process, has been used to fabricate TiNi products for medical implants or actuators [3−8]. In the SLM process, spherical TiNi powders produced by gas atomization were used as the raw feedstock. Since SLM involves very high localized temperature, the characteristics of raw powders play an important role in determining the microstructure and properties of the additively manufactured (AMed) products. For instance, LI et al [8] found that the Ti_2Ni secondary phase originally from the raw TiNi powders retained in the AMed sample after SLM; some defects or pores in the AMed sample are also thought to inherit from the raw powders. YABLOKOVA et al [9] also found that particle size, shape, size distribution and surface properties of the feedstock powders affect the powder flowability and processing conditions for SLM. Therefore, a thorough characterization of the starting TiNi powders in terms of microstructure, particle size and shape, and martensitic transformation temperature provides critical information about the technical operation and the attained AMed

Foundation item: Project (2016KJXX-78) supported by the Shaanxi Youth Science and Technology New Star Project, China; Project (2016KTCQ01-113) supported by the Shaanxi Science and Technology Co-ordination and Innovation Project, China; Project (51604228) supported by the National Natural Science Foundation of China; Project supported by the Open Fund of State Key Laboratory for Powder Metallurgy, Central South University, China
Corresponding author: Hui-ping TANG; Tel: +86-29-86231095; Fax: +86-29-86264926; E-mail: hptang@c-nin.com
DOI: 10.1016/S1003-6326(17)60293-0

engineering products.

In addition to gas atomization, plasma rotating electrode process (PREP) is also a widely used technique to produce spherical powders with high sphericity, low porosity and low interstitials [10−13]. In the PREP set-up, the pre-alloyed TiNi ingot is the electrode. An argon plasma arc is used to melt the rapidly rotating TiNi electrode and molten droplets are spun off and then solidified to form spherical particles in flight in the argon atmosphere [12]. In general, PREP is a rapid cooling process and therefore the high temperature phases can be retained to room temperature. The cooling rate in each individual particle is different, depending on its particle size. Therefore, the phase constituents in various particles might be different. For example, BASAK et al [14] found some Ti_2Ni phase nano-particles co-existing with predominant *B*2-TiNi phase in the macro-sized powders. They speculated that the existence of Ti_2Ni is a result of an equilibrium eutectic reaction owing to the low cooling rate. Nevertheless, the clarification of the existence of secondary phases in the PREP NiTi powder is still lacking. On the other hand, if secondary phases do exist, the mechanism by which these secondary phases are formed is not well understood. BASAK et al [14] suggested that a possible correlation exists between particle size and phases presented in the particles. This study therefore aims to clarify such a correlation, using the PREP technique to produce spherical TiNi powders with a wide range of particle size. The objectives of this study are thereby to investigate the effect of particle size on the micro-morphology, phase constituent and martensitic transformation of the PREPed TiNi powders, and to explain the formation of secondary phases, if they are present.

2 Experimental

The pre-alloyed TiNi rods (48.7%Ti−51.3%Ni, mole fraction), 75 mm in diameter and 400 mm in length, were used as the rotating electrode. The oxygen level in the starting TiNi rod is 0.037% (mass fraction). The spherical TiNi powders were subsequently produced using a PREP atomizer (SLPREP-1, Sailong Metal Materials Co., Ltd., China) [13], as shown in Fig. 1. The entire experiment was performed in a high-purity argon atmosphere. The main PREP processing parameters in this study are shown in Table 1.

Afterwards, the powders were sieved into three batches with various particle size ranges, i.e., ≥178 μm

Table 1 Information for PREP processing parameters

Plasma gas	Rotational speed/(r·min^{-1})	DC current/A	Feeding rate/ (mm·min^{-1})
Ar (4N purity)	12000	1100	~1.3

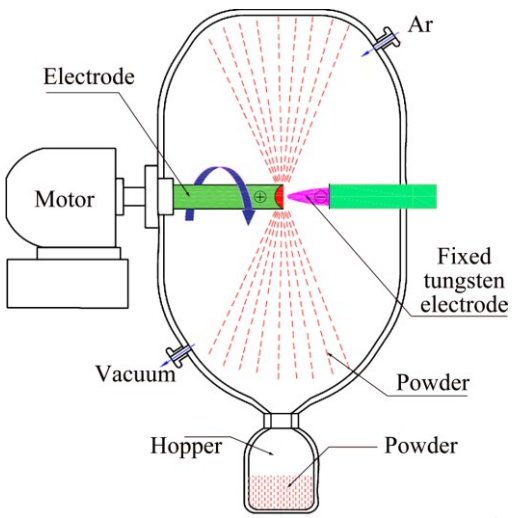

Fig. 1 Schematic of plasma rotating electrode process (PREP)

(denoted by TiNi-Coarse), 74−150 μm (TiNi-Med), ≤40 μm (TiNi-Fine), respectively. The flowability of the PREPed TiNi powders was determined according to the ASTM B213−13 standard with a Hall flowmeter, while their apparent density was determined as per the ASTM B212−13 standard. Phase constituents of the powders were determined by X-ray diffraction (XRD, Bruker D8 Advance Phaser) with Cu K_α radiation at room temperature. The X-ray diffraction (XRD) analysis was performed on a Bruker D8 Advance Phaser diffractometer at 40 kV with 2θ angle from 10° to 90°. To prepare the cross-section metallographic samples, the powder particles were mounted in epoxy resin, mechanically polished with SiC papers and finally etched with Kroll's reagent. Scanning electron microscopy (SEM, JEOL JSM−6460) equipped with energy-dispersive X-ray spectrometry (EDX) was used to characterize the surface and cross-sectional microstructures of powders. The interstitial contents were measured with an inert gas fusion analytical instrument (Leco TCH 600). Phase transformation temperatures of the TiNi powders were determined by differential scanning calorimetry (DSC, NETZSCH DSC 204F1) with a heating-and-cooling rate of 10 K/min between −120 and 150 °C.

To investigate the effect of cooling rate on the phase transformation of TiNi during cooling, disk samples of 20 mm in diameter and 5 mm in thickness, cut from the starting TiNi rod were heated to 660 °C, held at this temperature for 0.5 h and then quenched in water. The heating and quenching were conducted in a water-quenching vacuum furnace (vacuum level: 1×10^{-2} Pa). Another experiment was carried out with the same heat profile but followed by furnace cooling instead of water-quenching. In recent work, CHEN et al [15−18]

used in-situ neutron diffraction to confirme that there exists a eutectoid decomposition of TiNi → Ti_2Ni + Ni_3Ti at 630 °C if samples are furnace- cooled from the single-phase region. However, if the cooling rate is sufficiently high, the eutectoid reaction should be suppressed, thus yielding no secondary phases. Hence, we chose 660 °C as the heat treatment temperature to achieve a starting single phase, which was then subjected to various cooling rates. The information obtained from these heat treatment experiments were then fed back to investigate the relationship between the particle size and phase constituents in the PREPed TiNi powder.

3 Results and discussion

3.1 TiNi powders by PREP

Figure 2 shows the features of the edge and surface of the TiNi anode after PREP. It can be seen that the edge and cross-section surfaces of the anode are smooth. According to CHAMPAGNE and ANGERS [19], the melt flows to the edge of anode as a consequence of the centrifugal force, forming an earring that is further disintegrated into liquid droplets, which are solidified into "primary particles", as shown in Fig. 2(c). The large liquid droplets may be further disintegrated into smaller ones, which are solidify into the so-called "secondary particles". Due to surface tension during rapid solidification, spherical or spheroid particles are formed [14,19−21]. The atomizing mechanisms involved in PREP include direct drop formation (DDF), ligament disintegration (LD), and film disintegration (FD) [19].

The morphology of the PREPed TiNi powders without sieving is shown in Fig. 3(a). Most of the powders exhibit high sphericity and "satellite" powders can be rarely observed, which contributes to a good flowability of 19.7 s/(50 g) (Table 2). As displayed in Fig. 3(b), the particle size ranges from 40 to 180 μm with a typical bimodal distribution, which is thought to be a result of the DDF mechanism [19]. Moreover, the resulting particle size primarily depends on the operation parameters such as rotating speed, electrode diameter and DC current [22]. The apparent density and oxygen content of the PREPed powders (below 100 μm) is 4.03 g/cm^3 and 0.036%, respectively (Table 2).

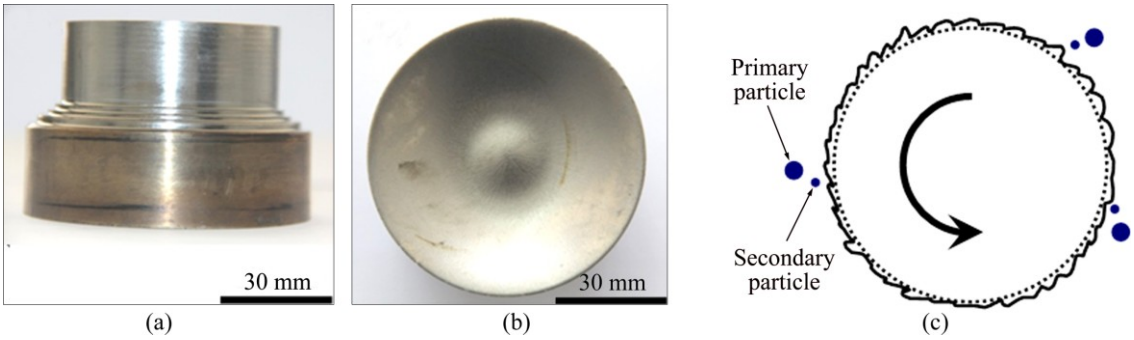

Fig. 2 Edge (a) and surface (b) of TiNi anode after PREP operation, and schematic illustration (c) of ideal process of droplets formation [19]

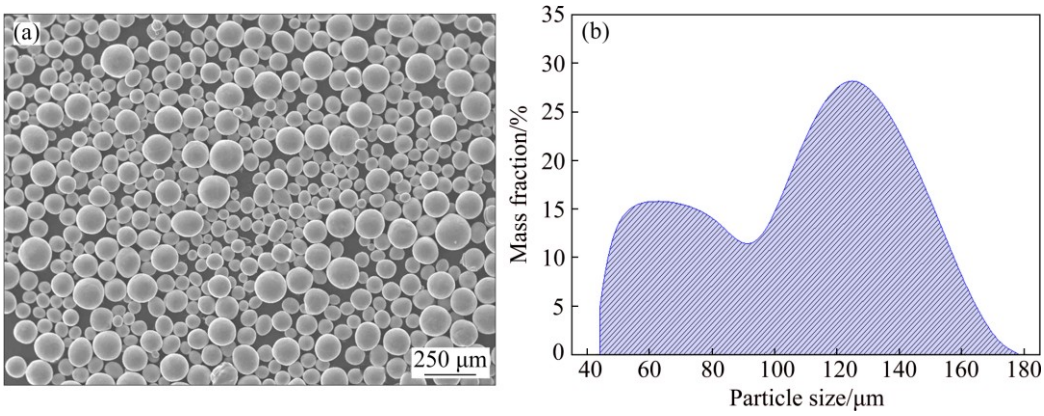

Fig. 3 Micro-morphology (a) and particle size distribution (b) of PREPed TiNi powders

Table 2 Basic characteristics of TiNi powders (<100 μm) produced by PREP

Parameter	Flowability/(s·(50 g)$^{-1}$)	Apparent density/(g·cm^{-3})	Oxygen content/%
Value	19.7	4.03	0.036

3.2 Effect of particle size on microstructure

A detailed observation of micro-morphologies of the powders is presented in Figs. 4 and 5. Figure 4 displays surface morphologies of the PREPed powders as a function of particle size. The particle surface becomes smoother and the grain structure becomes finer gradually as the particle size decreases, as shown in Figs. 4(b), (d) and (f). With respect to large particles such as the ones shown in Figs. 4(a) and (c), typical dendritic solidification morphology is observed. The dendritic feature becomes less obvious if the particle size is <40 μm, as presented in Fig. 4(f). This is mainly attributed to various cooling rates of powders associated with the particle size. It has been reported that the typical cooling rate of PREPed titanium powders is estimated to be 10^4−10^6 K/s [23], depending on particle size. With increasing cooling rate, the dendrites are gradually inhibited [10,20,24,25]. At extremely high cooling rates, even the cells (i.e., dendrites without secondary arms) may be completely suppressed, forming a featureless

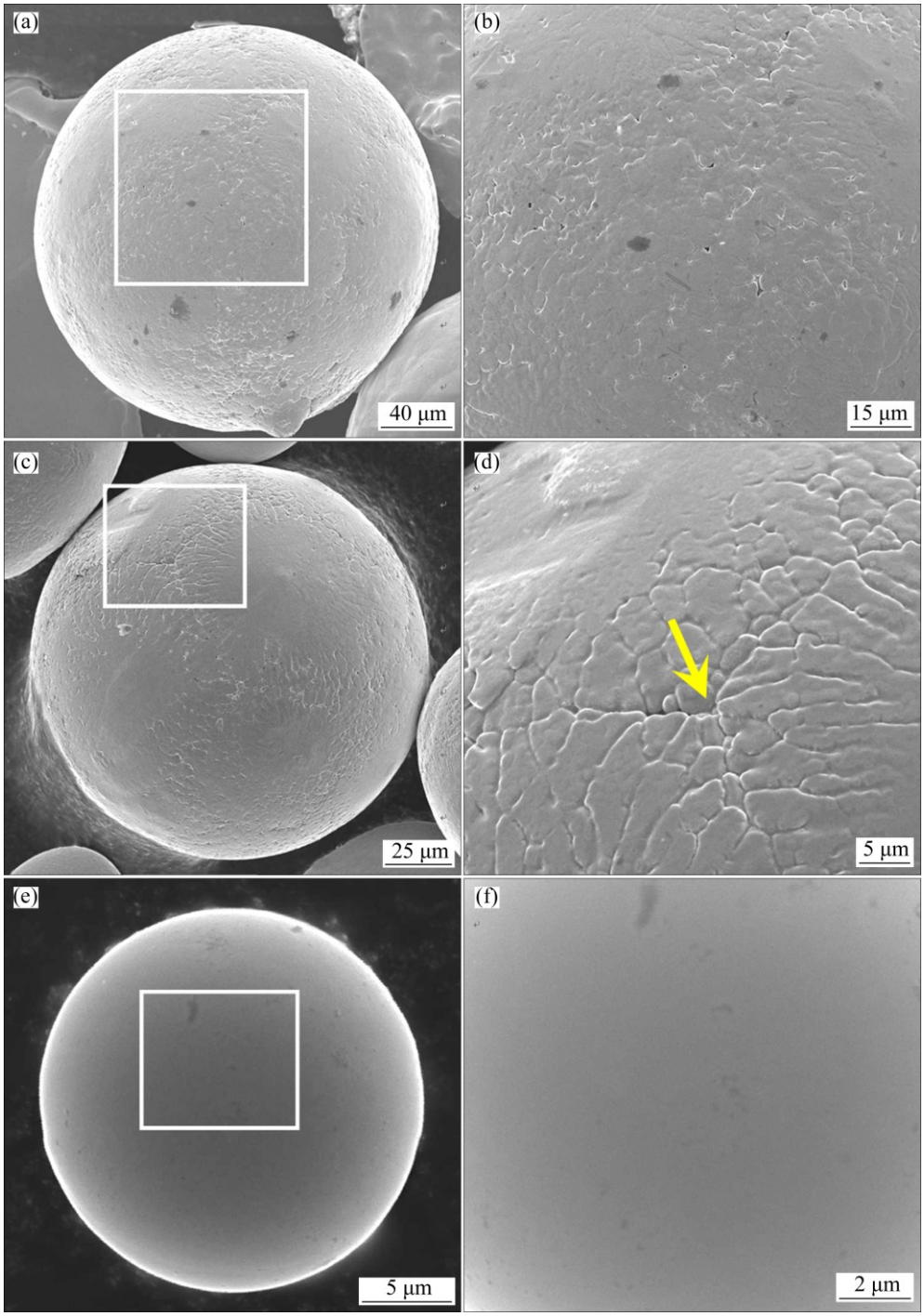

Fig. 4 Surface morphologies of PREPed TiNi powders with different particle sizes: (a, b) ≥178 μm (TiNi-Coarse); (c, d) 74−150 μm (TiNi-Med); (e, f) ≤40 μm (TiNi-Fine)

microstructure. Therefore, smaller particles yield smoother surface without any visible feature, e.g., Fig. 4(f). However, crystallization features can be obviously seen on the surface of larger particles (Figs. 4(b) and (d)). The arrow in Fig. 4(d) may indicate an intersection point of grain boundaries formed on its surface during rapid solidification.

The microstructures observed on the cross-sections are illustrated in Fig. 5. A small particle size corresponds to a fine-grained microstructure (Fig. 5). For example, the average grain size is approximately 3 μm in the intermediate sized particles (TiNi-Med powder in Fig. 5(d)). It is interesting from Figs. 5(e) and (f) that the phase constituent in smaller particles is TiNi phase. Detailed discussion of phase constituents in powders with various particle sizes will be given in the following section.

3.3 Effect of cooling rate on phase constituents

Figure 6 [26] shows the phase constituents of the PREPed TiNi powders with different particle sizes determined by XRD. The pattern of the starting material

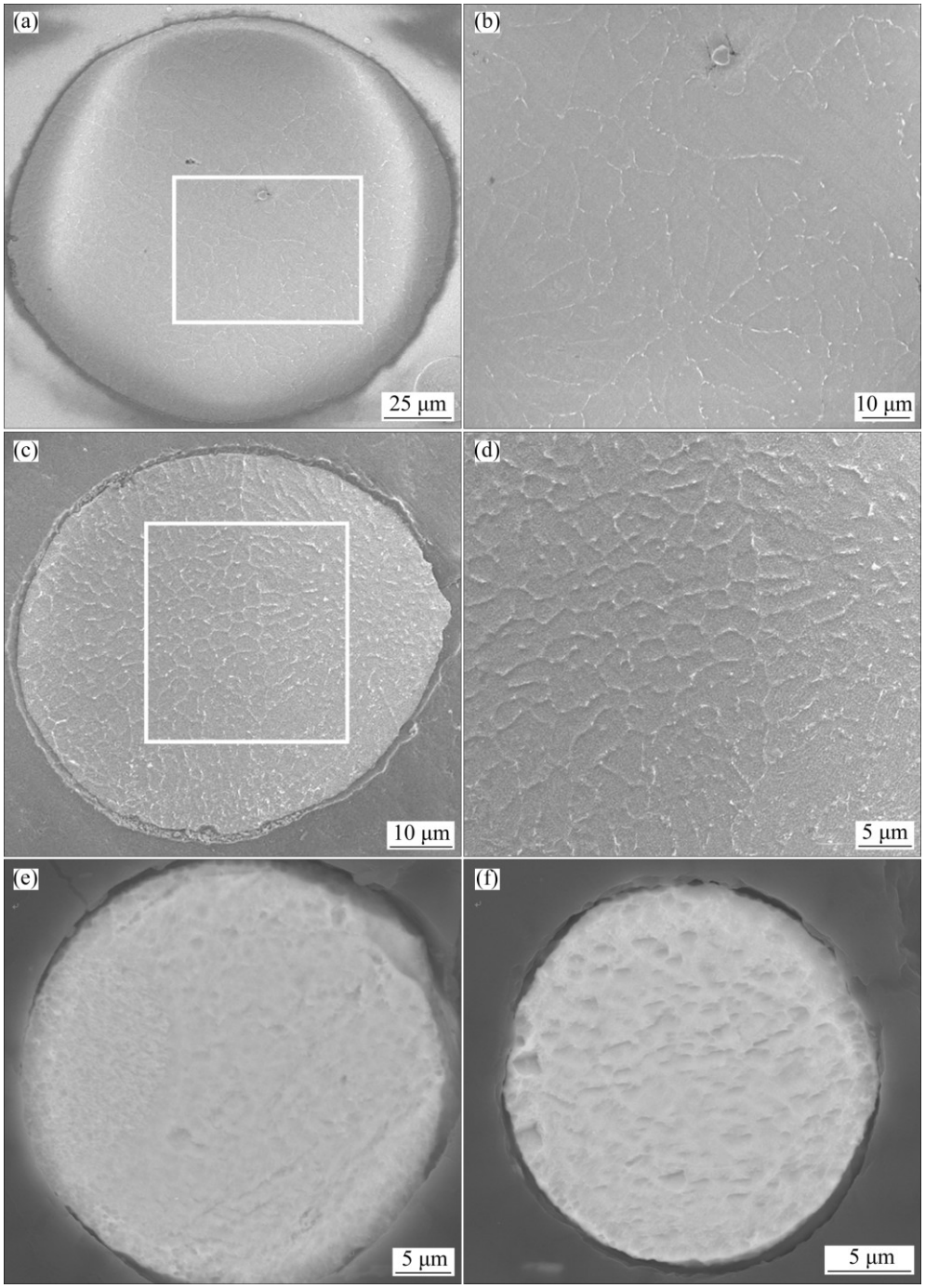

Fig. 5 Cross-sectional microstructures of various TiNi particles: (a, b) ~190 μm; (c, d) ~90 μm; (e) ≤40 μm; (f) ≤20 μm

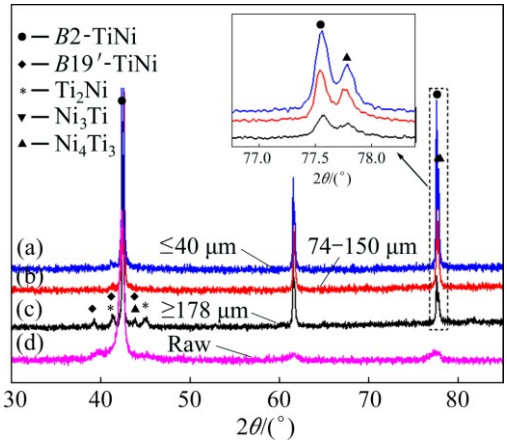

Fig. 6 XRD patterns of raw material and PREPed TiNi powders with various particle sizes [26]

is also presented in Fig. 6(d), showing a single *B*2-TiNi phase. In contrast, the powders demonstrate other phase constituents, although the main phase is still the *B*2-TiNi phase (Figs. 6(a)−(c)). Particularly, large particles with the size ≥178 μm exhibit additional minor secondary phases, i.e., Ti_2Ni, Ni_3Ti and Ni_4Ti_3 (see Fig. 6(c)). Table 3 summarizes the phase compositions of the raw TiNi rod and PREPed powders with various particle sizes. TiNi, Ni_3Ti and Ti_2Ni phases were confirmed by EDX analysis, while the Ni_4Ti_3 phase was not detected by EDX since it was too small in either size or quantity. Different from large particles, smaller powders (with the particle size of 74−150 μm and ≤40 μm) only show the *B*2-TiNi and Ni_4Ti_3 phases as shown in Figs. 6(a), (b) and Table 3.

Table 3 Phase compositions of raw material and PREPed powders

Sample size	Phase composition
Raw material	*B*2-TiNi
≥178 μm	*B*2-TiNi, Ti_2Ni, Ni_3Ti, Ni_4Ti_3, *B*19′-TiNi
74−150 μm	*B*2-TiNi, Ni_4Ti_3
≤40 μm	*B*2-TiNi, Ni_4Ti_3

According to the binary Ti−Ni phase diagram in Fig. 7 [26], the small amount of secondary Ni_3Ti and Ti_2Ni detected by XRD for the particles above 178 μm (Fig. 6(c)) is therefore possibly attributed to eutectoid decomposition of NiTi → $NiTi_2$ + Ni_3Ti at 630 °C. Although the liquid melt would rapidly be solidified into the *B*2-NiTi phase, the cooling process in large particles from *B*2 phase might be slowed so that the eutectoid phases $NiTi_2$ and Ni_3Ti are readily formed. The persistent eutectoid reaction has been confirmed in the works by CHEN et al [15−18]. If the particles are small, the cooling from *B*2 phase is expected to be sufficiently rapid, thus suppressing the eutecoid decomposition.

To further confirm our speculation and investigate the effect of cooling rate on the phase transformation during cooling, bulk TiNi samples cut from the raw rod were subjected to a water-quenching and a furnace-cooling heat treatment, respectively. As illustrated in the experimental section, one batch of disk samples was first heated to 660 °C (well above 630 °C) and held for 0.5 h in a vacuum furnace, followed by water quenching. The other batch was subjected to the same heating treatment but followed by furnace cooling. Figure 8 shows the XRD patterns of bulk samples after the two heat treatments. Only the *B*2-TiNi phase is observed in the water-quenched sample (Figs. 8(a) and (c)). On the contrary, as shown in Fig. 8(b), the phases observed after furnace cooling from 660 °C include *B*2-TiNi, Ni_3Ti and Ti_2Ni. This suggests that different cooling rates result in diverse phases or phase transformations, although both experiments used the identical raw material. Again, this further proves that the eutectoid reaction of TiNi → Ni_3Ti + Ti_2Ni at 630 °C (Fig. 7) is inhibited by water quenching due to very high cooling rate, while this

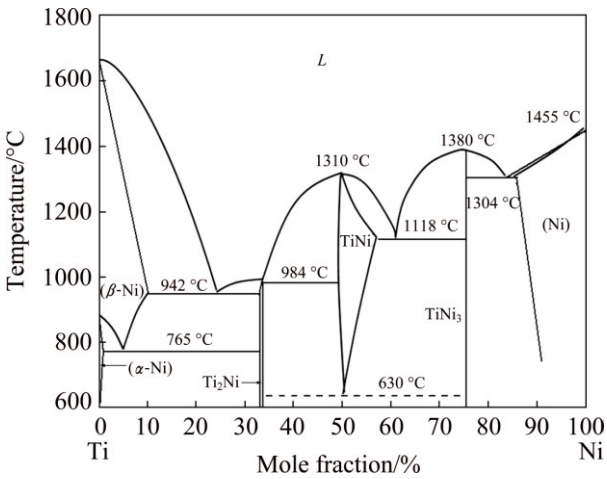

Fig. 7 Ti−Ni binary phase diagram (Redrawn from Ref. [26])

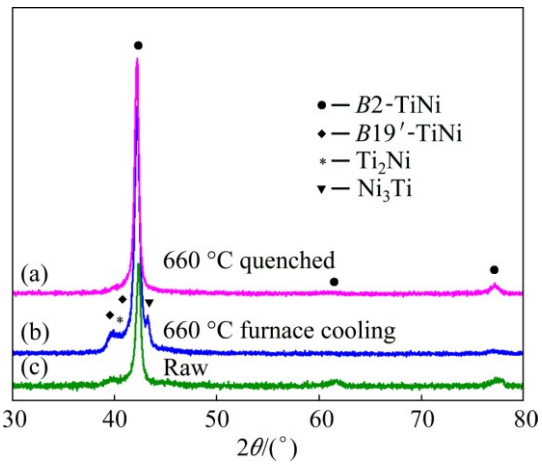

Fig. 8 XRD patterns of raw TiNi sample and TiNi bulk samples conducted after furnace cooling and vacuum water quenching

reaction is inevitable during furnace cooling. Therefore, this result agrees well with the previous analysis, confirming the effect of cooling rate on the eutectoid reaction at 630 °C, leading to different phase constituents. This further indicates that the existence of Ni_3Ti and Ti_2Ni secondary phases in large powders is most possibly owing to the eutectoid decomposition of TiNi → Ni_3Ti + Ti_2Ni at 630 °C during cooling. BASAK et al [14] also observed nano-sized Ti_2Ni particles co-existing with predominant *B*2-TiNi phase in the macro-sized PREPed Ni−Ti−Fe powders. They also speculated that the existence of Ti_2Ni is a result of an equilibrium eutectic reaction owing to its low cooling rate. It needs to note that the mean particle size of the PREPed Ni−Ti−Fe macro-powders in Ref. [14] was much larger, i.e., 400 μm, than that of powders in this study. Nevertheless, the eutectoid reaction of TiNi→ Ni_3Ti+Ti_2Ni at 630 °C should be more likely to occur during rapid cooling in larger particles.

3.4 Effect of particle size on martensitic transformation temperature

Figure 9 presents DSC curves of the PREPed TiNi powders with various particle sizes upon cooling and heating. Additionally, phase transformation temperatures for powders analyzed from Fig. 9 are shown in Table 4. The peak temperatures of martensitic transformation (M_p) during cooling are 6, −43 and −68 °C for powders with the particle size ≥178 μm, 74−150 μm and ≤40 μm, respectively. Interestingly, two important observations can be drawn from Fig. 9 and Table 4. Firstly, the martensitic transformation temperature decreases with decreasing the particle size of powders. Secondly, powders above 178 μm undergo a one-step of *B*2→*B*19′ phase transformation during cooling, while smaller powders exhibit a two-step *B*2→*R*→*B*19′ martensitic transformation process.

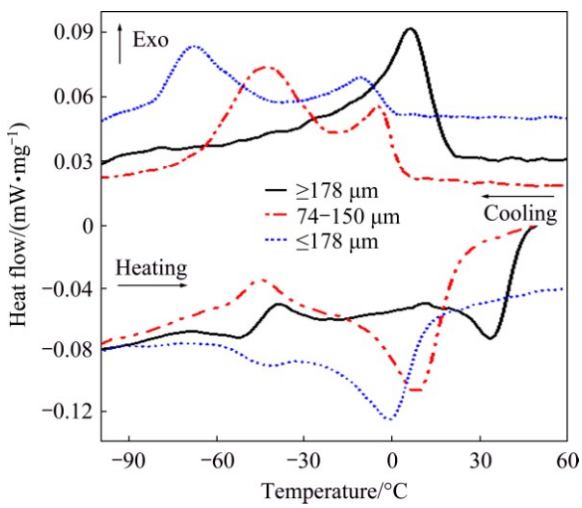

Fig. 9 DSC curves upon cooling and heating for PREPed TiNi powders with various particle sizes

Table 4 Phase transformation temperatures for PREPed TiNi powders with different particle sizes

Particle size/μm	A_s/ °C	A_p/ °C	A_f/ °C	R_s/ °C	R_p/ °C	M_s/ °C	M_p/ °C	M_f/ °C
≥178	20	33	44	−	−	19	6	−5
74−150	7	8	23	3	−6	−20	−43	−67
≤40	−26	−1	12	0	−11	−39	−68	−79

A_s, A_p, A_f, R_s, R_p, M_s, M_p and M_f represent temperatures of austenite start, austenite peak, austenite finish, *R* phase start, *R* phase peak, martensite start, martensite peak and martensite finish, respectively

The crystal structures of the *B*2, *R* and *B*19′ phases are cubic, trigonal and monoclinic [27], respectively. In addition to the *B*2 and *B*19′ phases, the *R* phase is a commensurate phase that arises under certain conditions prior to transforming to the *B*19′ phase. *B*2→*R* transformation is also a martensitic transformation process, which competes with *B*2→ *B*19′ transformation. If the *B*2→*B*19′ transformation occurs first, the *B*2→*R* transformation is suppressed. MIYAZAKI and OTSUKA [28] summarized a few factors effective to depress the martensite start temperature (M_s) and to favor the *R* phase formation: 1) substitution of a third element such as Fe or Al in the TiNi alloys; 2) the precipitation of Ti_3Ni_4 (*R*) phase after aging heat treatment; and 3) introduction of dislocations. WAITZ et al [29] observed that the *B*2→*B*19′ martensitic transformation is suppressed by decreasing grain size in a Ni−50.3%Ti alloy; M_s drops below the transformation temperature of the *R* phase if the grain size is < 150 nm. This leads to a two-step transformation from *B*2 to *B*19′ via the *R* phase. Our results also support that the grain refinement suppresses the martensitic transformation.

In addition, the existence of secondary phases, i.e., Ni_3Ti and Ti_2Ni (Fig. 6(c)) in large powders may favor the one-step *B*2→*B*19′ martensitic transformation, as shown in Fig. 9. It is interesting to note that the reverse martensitic transformation is only one-step *B*19′→*B*2 transformation for all the TiNi powders (Fig. 9), indicating that reverse *R* phase transformation and reverse martensitic transformation are overlapped [30,31]. This phenomenon has been analyzed systematically by REN et al [27,32,33].

It needs to point out the effect of Ni content on the martensitic transformation temperature [27,34]. In particular, with 0.1% (mole fraction) variation in Ni content the martensitic transformation temperature could change by about 10 °C [34].

4 Conclusions

1) The cooling rate of TiNi powders varies with particle size. Due to various cooling rates, coarser powders exhibit dendritic solidification morphology,

while finer powders achieve much smoother surface and finer grain size.

2) Powders with smaller particle size (74−150 μm and ≤40 μm) demonstrate the *B*2-TiNi and Ti_3Ni_4 phases, while larger powders above 178 μm show *B*2-TiNi as the main phase plus minor Ni_3Ti and Ti_2Ni secondary phases most possibly owing to the eutectoid decomposition of TiNi → Ni_3Ti + Ti_2Ni at 630 °C during cooling.

3) The martensitic transformation temperature of TiNi powders decreases with decreasing particle size. In larger powders (≥178 μm) a one-step martensitic transformation (*B*2→*B*19′) occurs, while in smaller ones (74−150 μm and ≤40 μm) a two-step of *B*2→*R*→*B*19 path takes place. The suppression of one-step *B*2→*B*19′ martensitic transformation is mainly caused by grain refinement, as a result of rapid cooling.

Acknowledgements

The authors acknowledge the support from Hunan ACME Co., Ltd., China, for providing the water-quenching vacuum furnace used in this work. We also thank Mr. Lei SHEN at Northwest Institute for Non-ferrous Metal Research for his technical assistance.

References

[1] BUEHLER W J, GILFRICH J V, WILEY R C. Effect of low-temperature phase changes on mechanical properties of alloys near composition TiNi [J]. Journal of Applied Physics, 1963, 34: 1475−1477.

[2] YAMAUCHI K, OHKATA I, TSUCHIYA K, MIYAZAKI S. Shape memory and superelastic alloys: technologies and applications [M]. Cambridge: Woodhead Publishing, 2011.

[3] BORMANN T, SCHUMACHER R, MÜLLER B, MERTMANN M, WILD M. Tailoring selective laser melting process parameters for NiTi implants [J]. J Mater Eng Perform, 2012, 21: 2519−2524.

[4] HABIJAN T, HABERLAND C, MEIER H, FRENZEL J, WITTSIEPE J, WUWER C, GREULICH C, SCHILDHAUER T A, KÖLLER M. The biocompatibility of dense and porous nickel–titanium produced by selective laser melting [J]. Materials Science and Engineering C, 2013, 33: 419−426.

[5] DADBAKHSH S, SPEIRS M, KRUTH J P, HUMBEECK J V. Influence of SLM on shape memory and compression behaviour of NiTi scaffolds [J]. CIRP Annals: Manufacturing Technology, 2015, 64: 209−212.

[6] DADBAKHSH S, VRANCKEN B, KRUTH J P, LUYTEN J, van HUMBEECK J. Texture and anisotropy in selective laser melting of NiTi alloy [J]. Materials Science and Engineering A, 2016, 650: 225−232.

[7] KHADEMZADEH S, CARMIGNATO S, PARVIN N, ZANINI F, BARIANI P F. Micro porosity analysis in additive manufactured NiTi parts using micro computed tomography and electron microscopy [J]. Materials & Design, 2016, 90: 745−752.

[8] LI S, HASSANIN H, ATTALLAH M M, ADKINS N J E, ESSA K. The development of TiNi-based negative Poisson's ratio structure using selective laser melting [J]. Acta Materialia, 2016, 105: 75−83.

[9] YABLOKOVA G, SPEIRS M, HUMBEECK J V, KRUTH J P, SCHROOTEN J, CLOOTS R, BOSCHINI F, LUMAY G, LUYTEN J. Rheological behavior of *β*-Ti and NiTi powders produced by atomization for SLM production of open porous orthopedic implants [J]. Powder Technology, 2015, 283: 199−209.

[10] SURYANARAYANA C, FROES F H, ROWE R G. Rapid solidification processing of titanium alloys [J]. International Materials Reviews, 1991, 36: 85−123.

[11] FROES F H. Powder metallurgy of titanium alloys [M]. Cambridge: Woodhead Publishing, 2013.

[12] NEIKOV O D, NABOYCHENKO S S, MURASHOVA I V, GOPIENKO V G, FRISHBERG I V, LOTSKO D V. Handbook of Non-ferrous Metal Powders [M]. Oxford: Elsevier, 2009.

[13] YIN J O, CHEN G, ZHAO S Y, GE Y, LI Z F, YANG P J, HAN W Z, WANG J, TANG H P, CAO P. Microstructural characterization and properties of Ti−28Ta at.% powders produced by plasma rotating electrode process [J]. Journal of Alloys and Compounds, 2017, 713: 222−228.

[14] BASAK C B, KRISHNAN M, KUMAR R, ABDULLAH K K, ANANTHARAMAN S. Characterization and process evaluation of Ni−Ti−Fe shape memory alloy macro-spheres directly fabricated via rotating electrode process [J]. Journal of Alloys and Compounds, 2014, 597: 15−20.

[15] CHEN G, LISS K D, CAO P. In situ observation and neutron diffraction of NiTi powder sintering [J]. Acta Materialia, 2014, 67: 32−44.

[16] CHEN G, LISS K D, CAO P. In situ observation of phase transformation of powder sintering from Ni/TiH_2 using neutron diffraction [C]//TMS 2014 Supplemental Proceedings. New York: John Wiley & Sons, Inc., 2014: 967−973.

[17] CHEN G, LISS K D, CAO P. An in situ study of NiTi powder sintering using neutron diffraction [J]. Metals, 2015, 5: 530−546.

[18] CHEN G, LISS K D, CAO P. An In situ study of sintering behavior and phase transformation kinetics in NiTi using neutron diffraction [J]. Metallurgical and Materials Transactions A, 2015, 46: 5887−5899.

[19] CHAMPAGNE B, ANGERS R. REP (rotating electrode process) atomization mechanisms [J]. Powder Metall Int, 1984, 16: 125−128.

[20] YANG D Y, GUO S, PENG H X, CAO F Y, LIU N, SUN J F. Size dependent phase transformation in atomized TiAl powders [J]. Intermetallics, 2015, 61: 72−79.

[21] ZDUJIĆ M, USKOKOVIĆ D. Production of atomized metal and alloy powders by the rotating electrode process [J]. Powder Metall Met Ceram, 1990, 29: 673−683.

[22] HATA S, OKI K, HASHIMOTO T, KUWANO N. Microstructures of Ti50Al45Mo5 alloy powders produced by plasma rotating electrode process [J]. Journal of Phase Equilibria, 2001, 22: 386−393.

[23] BRODERICK T F, JACKSON A G, JONES H, FROES F H. The effect of cooling conditions on the microstructure of rapidly solidified Ti−6Al−4V [J]. Metallurgical Transactions A, 1985, 16: 1951−1959.

[24] NISHIDA M, TATEYAMA T, TOMOSHIGE R, MORITA K, CHIBA A. Electron microscopy studies of Ti−47 at. % Al powder produced by plasma rotating electrode process [J]. Scripta Metallurgica et Materialia, 1992, 27: 335−340.

[25] DIXON C F. Atomizing molten metals—A review [J]. Canadian Metallurgical Quarterly, 1973, 12: 309−322.

[26] MASSALSKI T B, OKAMOTO H, SUBRAMANIAN P R, KACPRZAK L. Binary alloy phase diagrams [M]. 2nd ed. Ohio: ASM International, 1990.

[27] OTSUKA K, REN X. Physical metallurgy of Ti−Ni-based shape memory alloys [J]. Progress in Materials Science, 2005, 50: 511−678.

[28] MIYAZAKI S, OTSUKA K. Deformation and transition behavior associated with the *R*-phase in Ti−Ni alloys [J]. Metallurgical Transactions A, 1986, 17: 53−63.

[29] WAITZ T, KAZYKHANOV V, KARNTHALER H P. Martensitic phase transformations in nanocrystalline NiTi studied by TEM [J]. Acta Materialia, 2004, 52: 137−147.

[30] WAITZ T. The self-accommodated morphology of martensite in nanocrystalline NiTi shape memory alloys [J]. Acta Materialia, 2005, 53: 2273−2283.

[31] LIM Y G, HAN S H, CHOI E S, KIM W J. Enhancement of recovery stresses of the Ni−50.2Ti alloy by severe plastic deformation using a high-ratio differential speed rolling technique [J]. Scripta Materialia, 2016, 124: 95−98.

[32] REN X, MIURA N, TANIWAKI K, OTSUKA K, SUZUKI T, TANAKA K, CHUMLYAKOV Y I, ASAI M. Understanding the martensitic transformations in TiNi-based alloys by elastic constants measurement [J]. Materials Science and Engineering A, 1999, 273−275: 190−194.

[33] REN X, MIURA N, ZHANG J, OTSUKA K, TANAKA K, KOIWA M, SUZUKI T, CHUMLYAKOV Y I, ASAI M. A comparative study of elastic constants of Ti−Ni-based alloys prior to martensitic transformation [J]. Materials Science and Engineering A, 2001, 312: 196−206.

[34] PORTER D A, EASTERLING K E, SHERIF M Y. Phase transformations in metals and alloys [M]. 3rd ed. Boca Raton: CRC Press, 2009.

等离子旋转电极雾化法制备增材制造用形状记忆 TiNi 粉末

陈 刚[1,2]，赵少阳[1]，谈 萍[1]，殷京瓯[1]，周 全[1,3]，
葛 渊[1]，李增峰[1]，王 建[1]，汤慧萍[1,4]，Peng CAO[5]

1. 西北有色金属研究院 金属多孔材料国家重点实验室，西安 710016；
2. 中南大学 粉末冶金国家重点实验室，长沙 410083；
3. 东北大学 材料科学与工程学院，沈阳 110819；
4. 西安赛隆金属材料有限责任公司，西安 710016；
5. Department of Chemical and Materials Engineering, The University of Auckland, Private Bag 92019, Auckland 1142, New Zealand

摘 要：利用等离子旋转电极雾化技术制备出增材制造用球形 TiNi 合金粉末。利用扫描电子显微镜、X 射线衍射和差示扫描量热法等分析手段对不同粒径的 TiNi 合金粉末表面及内部的显微组织、相组成和马氏体相变温度进行表征。实验结果表明，随着 TiNi 合金粉末粒度的逐渐减小，粉末表面的组织结构明显细化，且晶粒逐渐减小。另外，所有粒径的粉末以 *B*2-TiNi 相为主，且粒径≥178 μm 的粗颗粒粉末还含有少量 Ti_2Ni、Ni_3Ti 二次相。粗颗粒粉末内部少量二次相是在冷却过程中 TiNi 的共析反应产生的。在制粉过程中，不同粒度 TiNi 粉末的冷却速率不同。不同的冷却速率致使 TiNi 粉末的马氏体相变温度和马氏体相变路径不同。特别地，TiNi 粉末的相变温度随粉末粒径的减小而降低。

关键词：雾化；等离子旋转电极雾化；TiNi；粒度；马氏体相变

(Edited by Wei-ping CHEN)